Toward a Transportable Ca^+ Optical Clock with a Systematic Uncertainty of 4.8×10^{-18}

Mengyan Zeng,[1,2,3,‡] Yao Huang,[1,2,‡] Baolin Zhang,[1,2] Yanmei Hao,[1,2,4] Zixiao Ma,[1,2,4] Ruming Hu,[1,2,4] Huaqing Zhang,[1,2] Zheng Chen,[1,2,4] Miao Wang,[1,2] Hua Guan,[1,2,5,*] and Kelin Gao[1,2,†]

[1] *State Key Laboratory of Magnetic Resonance and Atomic and Molecular Physics, Innovation Academy for Precision Measurement Science and Technology, Chinese Academy of Sciences, Wuhan 430071, China*

[2] *Key Laboratory of Atomic Frequency Standards, Innovation Academy for Precision Measurement Science and Technology, Chinese Academy of Sciences, Wuhan 430071, China*

[3] *School of Physics, Huazhong University of Science and Technology, Wuhan 430074, China*

[4] *University of Chinese Academy of Sciences, Beijing 100049, China*

[5] *Wuhan Institute of Quantum Technology, Wuhan 430206, China*

(Received 21 September 2022; revised 6 March 2023; accepted 21 April 2023; published 1 June 2023)

We present the compact long-term nearly continuous operation of a room-temperature Ca^+-optical-clock setup towards a transportable clock, achieving an overall systematic uncertainty of 4.8×10^{-18} and an uptime rate of 97.8% over an 8-day period. The active liquid-cooling scheme is adopted, combined with precise temperature measurement with 13 temperature sensors both inside and outside the vacuum chamber to ensure the accurate evaluation of the thermal environment for the optical clock. The environmental temperature uncertainty is evaluated as 293.31(0.4) K, corresponding to a blackbody-radiation frequency-shift uncertainty of 4.6×10^{-18}, which is reduced more than twice compared to our previous work. Through frequency comparison of the room-temperature Ca^+ optical clock with a cryogenic Ca^+ optical clock, the overall uncertainty of the clock comparison is 7.5×10^{-18}, including a statistical uncertainty of 4.9×10^{-18} and a systematic uncertainty of 5.7×10^{-18}. This work provides a set of feasible implementations for high-precision transportable ion optical clocks.

DOI: 10.1103/PhysRevApplied.19.064004

I. INTRODUCTION

Optical clocks based on neutral atoms trapped in an optical lattice or single ions trapped with ion traps have been greatly improved in the past two decades [1–7]. At present, the systematic uncertainties of optical clocks referenced to Yb [3], Sr [2,4], Al^+ [5], Yb^+ [6], and Ca^+ [7] have reached the 10^{-18} level or below [5]. The uncertainties of these state-of-the-art optical clocks have all exceeded the best Cs fountain clocks by more than 1 order of magnitude [8], with promising applications ranging from the redefinition of the SI second [8,9] to testing of the general relativity [10,11], testing if fundamental constants vary through time and space [11–14], geoid measurements [15], etc. The Comité International des Poids et Mesures proposed a roadmap for the redefinition of the SI second in 2018, which clearly stated that it was necessary to develop a transportable optical clock with an uncertainty at the 10^{-18} level to measure the frequency ratios between optical clocks in different institutes, with uncertainties at the 10^{-18} level, to check the reproducibility of the optical clocks and their frequency comparisons [8]. Besides, in terms of geoid measurements, a transportable optical clock with an uncertainty at the 10^{-18} level is required to achieve a centimeter-level height-difference resolution [16]. This will surpass the resolution of the traditional geodetic measurement scheme and will demonstrate the advantages of the optical-clock-based geopotential measurement. However, it is challenging to realize a transportable high-performance optical clock. Many institutions all around the world are now carrying out research on transportable optical clocks [16–20]. Among them, transportable Sr and Ca^+ optical clocks assembled in car trailers with systematic uncertainties at the 10^{-17} level have been developed [17,19]. RIKEN of Japan developed a cryogenic transportable Sr optical lattice clock at 245 K to suppress the blackbody-radiation- (BBR) shift uncertainty, achieving a systematic uncertainty of 5.5×10^{-18} [16].

The Ca^+ ion is an ideal reference candidate for building a transportable optical clock. It has a relatively simple

*guanhua@apm.ac.cn
†klgao@apm.ac.cn
‡These authors contributed equally to this work.

level scheme, requiring fewer numbers of diode lasers with weaker power compared to the Al^+- and Yb^+-based optical clocks [5,6] and the Yb- and Sr-based optical lattice clocks [3,4], allowing for the building of a compact, low-cost, and reliable transportable optical clock [19,20]. The uncertainty of our previous transportable Ca^+-ion optical clock was 1.3×10^{-17}, which was limited by the BBR-shift uncertainty [19]. A liquid-nitrogen-cooled cryogenic Ca^+-ion optical clock has been built with a systematic uncertainty of 3.0×10^{-18} [7], but it is difficult to apply it as a portable optical clock at the moment. Therefore, reducing the uncertainty of the BBR shift at room temperature is an important goal for building 10^{-18}-level-uncertainty transportable Ca^+ optical clocks. Here, temperature stabilization of the thermal environment, precise temperature measurement, and evaluation schemes are introduced to reduce the temperature variation and improve the accuracy of temperature evaluation. The uncertainty of the BBR frequency-shift evaluation is then lowered to the 10^{-18} level, and a frequency comparison with an overall uncertainty of 7.5×10^{-18} is implemented for the verification of the uncertainty evaluation.

In addition to the uncertainty, the continuous operation ability is the other essential feature of an optical clock for redefining the second [8]. Here, we report on an over-one-week operation of a room-temperature Ca^+ optical clock with an improved uptime rate of over 95%, after optimization of the laser system and the control program. Compared to other ion-based optical clocks, one group reported the long-term quasicontinuous performance of an Yb^+ clock with 76% uptime for 25 days [21]. Regarding optical lattice clocks, Sr optical lattice clocks with uptime rates of 93% for 10 days [22] and 84% for 25 days [23] were reported, and the long-term operation of an ^{171}Yb optical lattice clock for half a year, including uptimes of 93.9% for the first 24 days [24], was reported.

II. EXPERIMENTAL APPARATUS

Here, we present a room-temperature Ca^+ optical clock with an optimized structure of the ion trap (Fig. 1) and miniaturized titanium vacuum chamber [Fig. 2(a)]. A diamond-wafer-based linear ion trap is introduced with low heating rates. The ion trap is built of a laser-machined 300-μm-thick diamond wafer, which is gold plated to generate the radio-frequency (rf) trap electrodes and dc compensation electrodes on the diamond surface. The distances between the trapped ion and rf electrodes are about 0.25 mm. The ion-trap wafer and polished titanium endcaps are mounted on the silver-plated oxygen-free copper support with high thermal conductivity, which is attached to an oxygen-free copper heat sink with most surfaces exposed to the external vacuum environment. The heating rates of the trap are measured to be less than 5 quanta/s in all directions [25]. With a probe time of about 80 ms, the thermal-motion-shift uncertainty due to the heating rates is as low as the 10^{-19} level.

The vacuum chamber has a volume of $0.28 \times 0.16 \times 0.19$ m^3 and is made of titanium alloy. To achieve a stable magnetic field environment for Ca^+, four layers

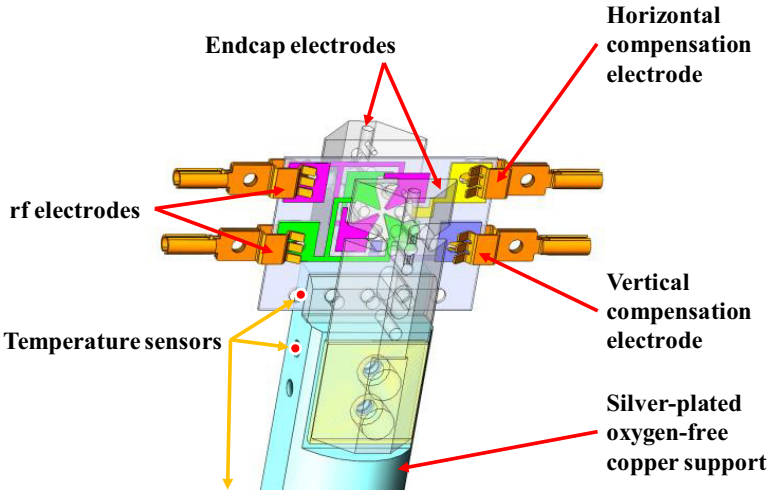

FIG. 1. Simplified schematic of the ion-trap system. Design is based on that used in NIST Al^+ clocks [5], with some minor modifications. Three in-vacuum thermocouple sensors with a calibration accuracy of 0.1 K are installed inside the vacuum chamber to characterize the thermal environment; one is installed at the diamond wafer to monitor its fluctuation, and two others are mounted on the top and middle of the silver-plated oxygen-free copper support to measure the temperature fluctuation and gradient of the vacuum chamber. Third thermocouple located in the middle of the support is not shown. Insulation materials between the endcap electrodes and copper support are also diamond. Design makes them nearly invisible to the ions, which means that the BBR-temperature uncertainty contributed by insulation supports is greatly suppressed.

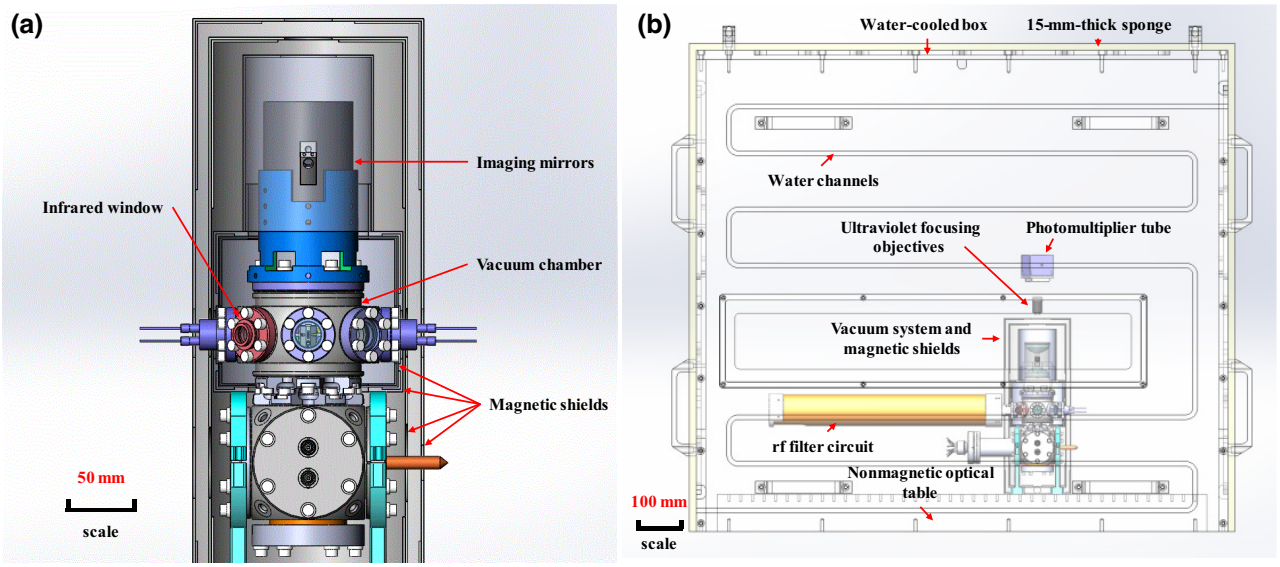

FIG. 2. (a) Vacuum chamber is made of titanium alloy to avoid the magnetic field produced by the chamber. Titanium-alloy material also helps to achieve higher vacuum. One CF35 window is on top for image collection and vertical laser probing, six CF16 windows are on the sides for laser cooling and probing in the corresponding directions, including an infrared window (colored in red) for the temperature measurement with an infrared camera, two CF16 feedthroughs are used for applying voltages on the trapping rf and compensation electrodes. Four layers of magnetic shields are added to significantly weaken the environmental magnetic field fluctuations. Within the magnetic shields, three pairs of coils are installed to adjust the strength and direction of the magnetic field. (b) Vacuum chamber is located in a liquid-cooled box to ensure uniformity and stability of the thermal environment. Brown tube is the helical resonator used for rf supply of the ion-trap system. Modules in the system are connected by optical fibers and cables with the laser-stabilization system and circuit control system in the laboratory environment.

of magnetic shields are added [Fig. 2(a)]. The vacuum chamber and optics are placed on a 0.9×0.7-m^2 table. The table is surrounded by a liquid-cooled box to isolate it from room-temperature fluctuations [Fig. 2(b)]. The size of the box is $1.14 \times 0.84 \times 1.03$ m^3. Ten platinum resistance-temperature detectors are installed to evaluate the thermal environment outside the vacuum chamber. The overall temperature-measurement system is calibrated with an accuracy level better than 0.1 K at the Hubei Institute of Measurement and Testing Technology. A detailed description of the liquid-cooled box is presented in Sec. 1 of the Supplemental Material [26].

Compared to the room-temperature optical clock, the vacuum system of our liquid-nitrogen cryogenic optical clock is relatively complex and huge [7]. Such a complex vacuum system is prone to vacuum leakage during transportation. Moreover, the current liquid-nitrogen Ca^+ optical clock requires daily liquid-nitrogen replenishment to maintain its operation, which prevents it from being transported long distances. In contrast to the cryogenic clock, the vacuum system of the room-temperature optical clock is relatively small and robust for easier transportation. Meanwhile, in the room-temperature optical clock, the liquid-cooled box is simply composed of five liquid-cooled panels, which can be easily disassembled and reassembled. In our preliminary test for transportation, the clock is moved from the 1-m-high optical table to the ground; it takes less than a day for the recovery of clock operation. Therefore, the room-temperature optical clock with our liquid-cooled scheme can be conveniently mounted in our transportable car trailer in the future.

III. FREQUENCY-SHIFT EVALUATION

Similar to our previously built optical clocks [7,25,27,38], cooling lasers under optimized operation conditions are adopted to reduce the second-order Doppler shift due to the secular motion of the ion. Considering the trap heating rates, the ion temperature is estimated as 1.19(33) mK during the clock-comparison experiments, corresponding to a second-order Doppler shift (due to secular motion) of $-(4.1 \pm 1.2) \times 10^{-18}$ [32–35]. The excess-micromotion-induced second-order Doppler shift and Stark shift, the combination of Stark shifts due to secular motion, and the second-order Doppler shift due to secular motion (micromotion induced) are canceled out by choosing the magic rf trapping frequency [27,32,36]. The excess-micromotion-induced shift and its uncertainty are evaluated to be less than 1×10^{-19}. The quadrupole shift, first-order Zeeman shift, and tensor Stark shifts due to ion motion and the lasers are canceled out by averaging the three pairs of Zeeman components [37,38]. A specific magnetic field direction is chosen to achieve a magic angle between the electric field gradient and the magnetic field direction for

TABLE I. Percentages of effective and geometric solid angles for different parts of the ion-trap system.

Vacuum part	Material	Emissivity	$\Omega_i^{\text{eff}}/(4\pi)$ (%)	$\Omega_i^{\text{geo}}/(4\pi)$ (%)
Endcaps	Titanium	0.166	47	51
Inner walls of vacuum chamber	Titanium	0.166	26	28
Ion trap (including compensation electrodes)	Gold	0.05	14	16
Glass window	Fused-silica glass	0.75	13	5

the reduction of the electric quadrupole shift drift, which greatly suppresses the residual quadrupole shift, with an evaluated uncertainty of 4×10^{-19} [39,40]. The servo shift and uncertainty are inferred from the small residual errors in the quantum jump imbalances recoded by the software [25,38]. The upper limit of the servo-induced frequency-shift uncertainty is evaluated to be 4×10^{-19}. In our experiment, two laser beams in opposite directions are used for independent and interleaved probing of the ion [5,7]. By averaging the two independent frequency measurements, the first-order Doppler shift is reduced with an uncertainty of 3×10^{-19}. The ac Stark shift due to the probe laser is greatly reduced with an uncertainty of $<1 \times 10^{-19}$ by adopting the hyper-Ramsey interrogation scheme [41,42]. More detailed methods and results of the evaluation of the systematic shifts and uncertainties are shown in Sec. 2 of the Supplemental Material [26]. After the abovementioned improvements and evaluations, for Ca^+ optical clocks, the total systematic uncertainty is mainly limited by the BBR shift.

For optical clocks, the BBR shift can be expressed as [43]

$$\Delta\nu_{\text{BBR}} = -\frac{\Delta\alpha_0}{2h}\langle E^2\rangle_T[1+\eta(T)] \tag{1}$$

where $\Delta\alpha_0$ is the differential static scalar polarizability for the clock transition, $\eta(T)$ is the dynamic correction coefficient, h is Plank's constant, and $\langle E^2\rangle_T = [8.319430(15)\ \text{V/cm}]^2(T/300\ \text{K})^4$ is the mean-squared electric field in a BBR environment at temperature T [44]. In our previous work, the differential static scalar polarizability, $\Delta\alpha_0$, was measured to be $-7.2677(21) \times 10^{-40}\ \text{J m}^2\ \text{V}^{-2}$ and the uncertainty of the BBR shift contributed by the BBR coefficient, $\Delta\alpha_0$, including dynamic correction, was reduced to 3×10^{-19} [27]. Therefore, the key to reducing the BBR frequency-shift uncertainty of the Ca^+ optical clock at room temperature is the suppression of BBR temperature uncertainty.

To estimate the blackbody-radiation temperature as accurately as possible, active temperature stabilization by liquid cooling, the precise measurement of the thermal environment, and finite-element (FE) analysis of the thermal radiation of the setups are implemented here. As Ca^+ is illuminated by the thermal radiation of the components of the ion-trap system, the effective BBR temperature, T_{eff}, felt by the ion can be calculated in terms of the effective solid angles and the temperatures of the surfaces of all components [28]:

$$T_{\text{eff}}^4 = \frac{c}{4\sigma}u = \sum_i \left(\frac{\Omega_i^{\text{eff}}}{4\pi}\right) T_i^4 \ , \tag{2}$$

where c is the speed of light, u is the local field energy density, and σ is the Stefan-Boltzmann constant. The radiating surface of each component of the trap system can be described by its own temperature, T_i, and the effective solid angle, Ω_i^{eff}, observed by the ions, and i runs over all enclosure surfaces. Ω_i^{eff} represents the weight of the corresponding part surface, i, when calculating T_i.

TABLE II. Temperature evaluation results for the ion-trap system.

Component	Temperature evaluation value (K)	Uncertainty due to sensor calibration (K)	Uncertainty due to temperature gradient (K)	Uncertainty due to ambient-temperature fluctuations (K)	Total uncertainty (K)
Endcaps	293.35	0.1	0.1	0.3	0.4
Inner walls of vacuum chamber	293.25	0.1	0.2	0.3	0.4
Ion trap (including compensation electrodes)	293.35	0.1	0.1	0.3	0.4
Glass window	293.25	0.1	0.2	0.3	0.4
T_{eff}	293.31				0.4

TABLE III. Systematic shifts and uncertainties for the evaluation of two clocks and their comparison. Here, only the effects with systematic shifts or uncertainties of $>1 \times 10^{-19}$ are shown.

Contributor (10^{-18})	Fractional systematic shift of clock 1 (10^{-18})	Fractional systematic uncertainty of clock 1 (10^{-18})	Fractional systematic shift of clock 2 (10^{-18})	Fractional systematic uncertainty of clock 2 (10^{-18})	Fractional systematic shift of clock 1-clock 2 (10^{-18})	Fractional systematic uncertainty of clock 1-clock 2 (10^{-18})
BBR-field evaluation (temperature)	842.8	4.6	7.3	2.7	835.5	5.3
BBR coefficient ($\Delta\alpha_0$)	0	0.3	0	0.3	0	0.4
Excess micromotion	0	0	0	0.2	0	0.2
Second-order Doppler (thermal)	−4.1	1.2	−3.1	0.9	−1	1.5
Residual quadrupole	0	0.4	0	0.4	0	0.6
Servo	0	0.4	0	0.4	0	0.6
First-order Doppler	0	0.3	0	0.3	0	0.4
Gravitational shift					−27.5	1
Total	838.7	4.8	4.2	3.0	807.0	5.7

Analysis of the BBR temperature based on the finite-element method shows that a large effective solid angle of the insulation supports, temperature fluctuation, and the gradient of the vacuum chamber typically give the largest contributions to the BBR temperature uncertainty [29,30]. The diamond-wafer-based linear ion-trap configuration makes the effective solid-angle contribution of the insulation supports almost disappear. Through active temperature control of the operating thermal environment of the optical clock by liquid cooling, the temperature fluctuation of the vacuum system is reduced from ±1.6 to ±0.3 K.

We calculate the effective solid angle of each component in the ion-trap system by FE analysis using a method similar to the one given in Ref. [7] with the COMSOL Multiphysics software. In the model, the calcium ion is replaced

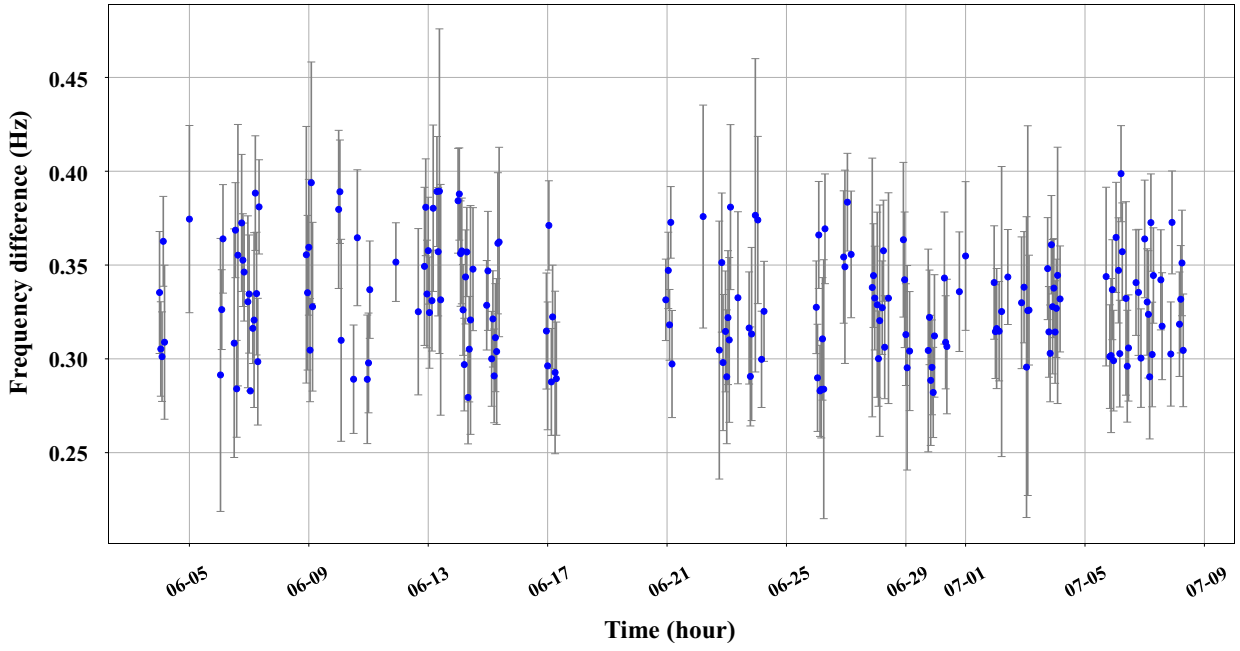

FIG. 3. Frequency comparison of the two clocks. Micromotion-minimization process is carried out and the ion temperature for the room-temperature clock is measured daily during the clock comparison. Frequency difference is measured to be 329.9 mHz with a statistical uncertainty of 2.0 mHz (4.9×10^{-18}). Combined with the systematic uncertainty of 5.7×10^{-18} described in Table II, the total uncertainty for the clock comparison is 7.5×10^{-18}. Uptime rate for the comparison is mainly limited by the cryogenic optical clock.

with a small blackbody sphere, which acts as a probe. Considering temperature control of the liquid-cooled box, the absolute temperatures of our vacuum parts, such as the vacuum chambers and ion trap, are very close to room temperature, effective solid angles, Ω_i^{eff}, in the case of a uniform temperature distribution can be used to characterize the realistic system [31]:

$$\frac{\Omega_i^{\text{eff}}}{4\pi} = \left(\frac{T_{\text{eff}}}{T_i}\right)^3 \frac{\partial T_{\text{eff}}}{\partial T_i} \tag{3}$$

where T_{eff} is the temperature of the probe and T_i is the set temperature for component i. In our case, $T_{\text{eff}}/T_i \approx 1$. Typical emissivity values are adopted for different surface materials in the calculations [29], the emissivity values of the endcaps, walls of the chamber, ion trap, and fused-silica windows are set to 0.166, 0.166, 0.05, and 0.75, respectively. For comparison, the geometric solid angles are also calculated using emissivity values of 1 for all surfaces. The results are listed in Table I. The temperature of different components can be measured by the temperature sensors combined with the infrared camera. The temperature-measurement details of each component are listed in Table II.

The effective BBR temperature felt by the ion is calculated to be 293.31(40) K, corresponding to a BBR-shift uncertainty of 1.9 mHz. Finally, the temperature-associated BBR shift uncertainty is determined to be 4.6×10^{-18}. It can be further reduced by calibrating the temperature sensor with an accuracy of less than 15 mK and designing a more uniform and stable temperature-control system for optical clocks.

Table III summarizes the systematic uncertainty budget for the room-temperature clock (clock 1 columns). The total systematic uncertainty is 4.8×10^{-18}; this is limited by the BBR temperature evaluation precision.

IV. CLOCK COMPARISON

We further measure the frequency difference between the room-temperature Ca^+-ion optical clock (clock 1 in Table III) and the cryogenic clock (clock 2 in Table III, with an uncertainty of 3.0×10^{-18}) [7] to verify the performance of the room-temperature clock. The two clocks have a height difference of 25(1) cm, corresponding to a frequency shift of 11.3(4) mHz or $27.5(1.0) \times 10^{-18}$ in fractional. In the frequency-comparison experiment, the same clock laser synchronously probes the two clocks to observe hyper-Ramsey spectroscopy with a free evolution time of 40 ms, and the frequency difference is obtained by comparing the two acousto-optic modulators used to modulate the two clock laser frequencies to make them resonant with the clock transitions. As shown in Table III, a fractional frequency-shift difference of $8.070(57) \times 10^{-16}$ is evaluated, corresponding to a 331.7(2.3)-mHz difference and a systematic uncertainty of 5.7×10^{-18}. As shown in Fig. 3, the measured frequency difference

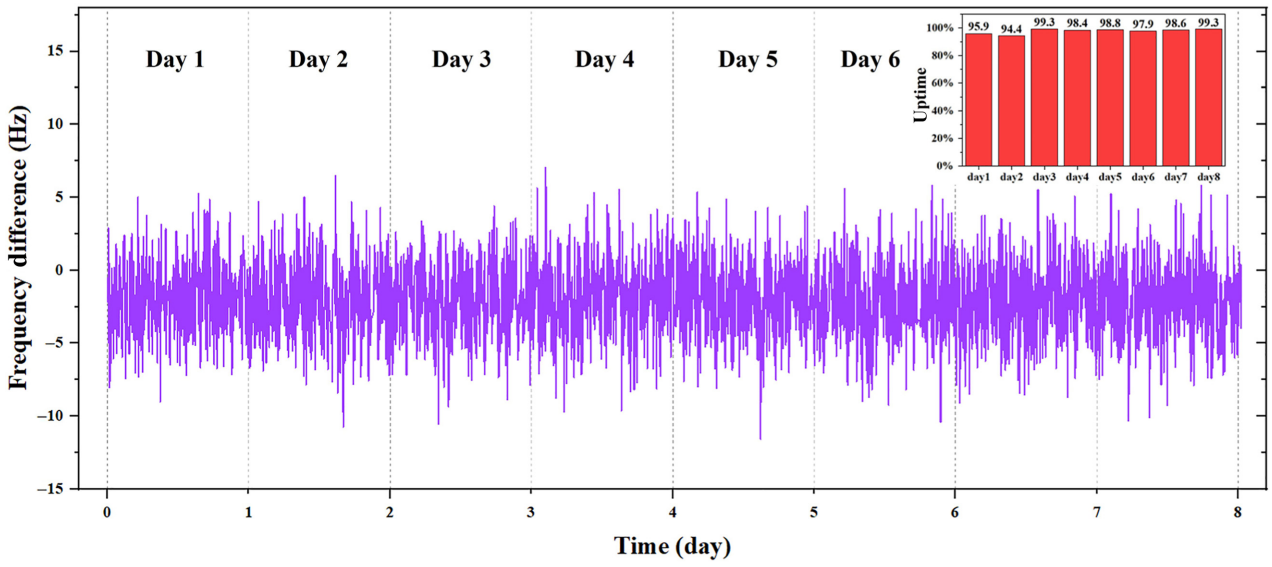

FIG. 4. Frequency difference between transition pairs $^2S_{1/2}(m=\pm1/2) \rightarrow {}^2D_{5/2}(m=\pm1/2)$ and $^2S_{1/2}(m=\pm1/2) \rightarrow {}^2D_{5/2}(m=\pm3/2)$ of the room-temperature clock. Rabi interrogation method with a 20-ms probe time is used. Operating uptime rate reaches 97.8% in a period of around 8 days. Current continuous uptime rate of the room-temperature clock is limited by ion loss caused by the instability of the frequency of the cooling laser and the interrogation operation of the probe laser, which occurs at a frequency of about once a day. Furthermore, unlocking of the clock laser would also cause operation of the optical clock to be interrupted. Future improvements will focus on reloading the $^{40}Ca^+$ ion faster and developing a more stable reference cavity for frequency stabilization of the clock laser.

is 329.9(2.0) mHz, which is in good agreement with the evaluated value. More details about the clock comparison, including the Allan deviation, are shown in Sec. 3 of the Supplemental Material [26].

V. UPTIME RATE OF THE CLOCK

The uptime rate of the room-temperature clock is measured, as shown in Fig. 4. The clock can reliably operate for over a week, with an uptime rate of over 95%. It is comparable to those optical clocks with long-term quasicontinuous performance, such as the Sr and Yb clocks mentioned in the end of Sec. I [22–24]. This experiment also verifies the reliability of the room-temperature optical clock after its preliminary transportation experiment from the optical table to the ground.

VI. CONCLUSION

We develop a nearly continuous Ca^+ optical clock towards a transportable clock, with a systematic uncertainty of 4.8×10^{-18} at room temperature. Through optimization of the ion-trap structure, the proportion of the effective solid angle of the insulating supports in the ion trap is greatly suppressed. Moreover, an active temperature control and evaluation scheme is introduced. These efforts help to reduce the portable Ca^+ optical clock's BBR-shift uncertainty to the 10^{-18} level. The evaluation is also verified by measuring the frequency difference between the room-temperature and cryogenic clocks with an overall uncertainty of 7.5×10^{-18}. This transportable Ca^+ optical clock achieves 10^{-18}-level systematic uncertainty and the Ca^+-optical-clock comparison shows 10^{-18}-level total uncertainty. Higher-accuracy clock comparisons can be implemented with optical clocks from other laboratories to test the uncertainty evaluation and measurements of clock-frequency ratios [45]. Our setups for reducing the BBR-shift uncertainty are suitable for developing robust transportable optical clocks based not only on Ca^+ ions, but also on other ions or neutral atoms.

ACKNOWLEDGMENTS

We thank Zhengtian Lu, Liyan Tang, Chaohui Ye, and Jun Luo for help and fruitful discussions. This work is supported by the National Key R&D Program of China (Grants No. 2022YFB3904001, No. 2022YFB3904004, and No. 2018YFA0307500), the National Natural Science Foundation of China (Grants No. 12022414 and No. 12121004), the Natural Science Foundation of Hubei Province (Grants No. 2022CFA013), the CAS Youth Innovation Promotion Association (Grants No. Y201963 and No. Y2022099), the CAS Project for Young Scientists in Basic Research (Grant No. YSBR-055), and the Interdisciplinary Cultivation Project of the Innovation Academy for Precision Measurement of Science and Technology (Grant No. S21S2201).

[1] A. A. Madej, P. Dubé, Z. Zhou, J. E. Bernard, and M. Gertsvolf, $^{88}Sr^+$ 445-THz Single-Ion Reference at the 10^{-17} Level via Control and Cancellation of Systematic Uncertainties and Its Measurement against the SI Second, Phys. Rev. Lett. **109**, 203002 (2012).

[2] I. Ushijima, M. Takamoto, M. Das, T. Ohkubo, and H. Katori, Cryogenic optical lattice clocks, Nat. Photonics **9**, 185 (2015).

[3] W. F. McGrew, X. Zhang, R. J. Fasano, S. A. Schäffer, K. Beloy, D. Nicolodi, R. C. Brown, N. Hinkley, G. Milani, M. Schioppo, *et al.*, Atomic clock performance enabling geodesy below the centimetre level, Nature **564**, 87 (2018).

[4] T. Bothwell, D. Kedar, E. Oelker, J. M. Robinson, S. L. Bromley, W. L. Tew, J. Ye, and C. J. Kennedy, JILA SrI optical lattice clock with uncertainty of 2.0×10^{-18}, Metrologia **56**, 065004 (2019).

[5] S. M. Brewer, J. S. Chen, A. M. Hankin, E. R. Clements, C. W. Chou, D. J. Wineland, D. B. Hume, and D. R. Leibrandt, $^{27}Al^+$ Quantum-Logic Clock with a Systematic Uncertainty below 10^{-18}, Phys. Rev. Lett. **123**, 033201 (2019).

[6] S. Dörscher, N. Huntemann, R. Schwarz, R. Lange, E. Benkler, B. Lipphardt, U. Sterr, E. Peik, and C. Lisdat, Optical frequency ratio of a $^{171}Yb^+$ single-ion clock and a ^{87}Sr lattice clock, Metrologia **58**, 015005 (2021).

[7] Y. Huang, B. Zhang, M. Zeng, Y. Hao, Z. Ma, H. Zhang, H. Guan, Z. Chen, M. Wang, and K. Gao, Liquid-Nitrogen-Cooled Ca^+ Optical Clock with Systematic Uncertainty of 3×10^{-18}, Phys. Rev. Appl. **17**, 034041 (2022).

[8] F. Riehle, P. Gill, F. Arias, and L. Robertsson, The CIPM list of recommended frequency standard values: Guidelines and procedures, Metrologia **55**, 188 (2018).

[9] P. Gill, Is the time right for a redefinition of the second by optical atomic clocks?, J. Phys.: Conf. Ser. **723**, 012053 (2016).

[10] T. Bothwell, C. J. Kennedy, A. Aeppli, D. Kedar, J. M. Robinson, E. Oelker, A. Staron, and J. Ye, Resolving the gravitational redshift across a millimetre-scale atomic sample, Nature **602**, 420 (2022).

[11] M. Takamoto, I. Ushijima, N. Ohmae, T. Yahagi, K. Kokado, H. Shinkai, and H. Katori, Test of general relativity by a pair of transportable optical lattice clocks, Nat. Photonics **14**, 411 (2020).

[12] A. Derevianko and M. Pospelov, Hunting for topological dark matter with atomic clocks, Nat. Phys. **10**, 933 (2014).

[13] P. Wcisło, P. Morzyński, M. Bober, A. Cygan, D. Lisak, R. Ciuryło, and M. Zawada, Experimental constraint on dark matter detection with optical atomic clocks, Nat. Astron. **1**, 0009 (2017).

[14] C. J. Kennedy, E. Oelker, T. Bothwell, D. Kedar, J. M. Robinson, W. Milner, G. E. Marti, and J. Ye, Precision Metrology Meets Cosmology: Improved Constraints on Ultralight Dark Matter from Atom-Cavity Frequency Comparisons, Phys. Rev. Lett. **125**, 201302 (2020).

[15] T. E. Mehlstäubler, G. Grosche, C. Lisdat, P. O. Schmidt, and H. Denker, Atomic clocks for geodesy, Rep. Prog. Phys. **81**, 064401 (2018).

[16] N. Ohmae, M. Takamoto, Y. Takahashi, M. Kokubun, K. Araki, A. Hinton, I. Ushijima, T. Muramatsu, T. Furumiya, Y. Sakai, *et al.*, Transportable strontium optical lattice clocks operated outside laboratory at the level of 10^{-18} uncertainty, Adv. Quantum Technol. **4**, 2100015 (2021).

[17] S. B. Koller, J. Grotti, S. Vogt, A. Al-Masoudi, S. Dörscher, S. Häfner, U. Sterr, and C. Lisdat, Transportable Optical Lattice Clock with 7×10^{-17} Uncertainty, Phys. Rev. Lett. **118**, 073601 (2017).

[18] S. Origlia, M. S. Pramod, S. Schiller, Y. Singh, K. Bongs, R. Schwarz, A. Al-Masoudi, S. Dörscher, S. Herbers, S. Häfner, U. Sterr, and C. Lisdat, Towards an optical clock for space: Compact, high-performance optical lattice clock based on bosonic atoms, Phys. Rev. A **98**, 053443 (2018).

[19] Y. Huang, H. Zhang, B. Zhang, Y. Hao, H. Guan, M. Zeng, Q. Chen, Y. Lin, Y. Wang, S. Cao, *et al.*, Geopotential measurement with a robust, transportable Ca^+ optical clock, Phys. Rev. A **102**, 050802 (2020).

[20] J. Cao, J. Yuan, S. Wang, P. Zhang, Y. Yuan, D. Liu, and K. Cui, A compact, transportable optical clock with 1×10^{-17} uncertainty and its absolute frequency measurement, Appl. Phys. Lett. **120**, 054003 (2022).

[21] C. F. A. Baynham, R. M. Godun, J. M. Jones, S. A. King, P. B. R. Nisbet-Jones, F. Baynes, A. Rolland, P. E. G. Baird, Kai Bongs, P. Gill, *et al.*, Absolute frequency measurement of the $^2S_{1/2} \rightarrow {}^2F_{7/2}$ optical clock transition in $^{171}Yb^+$ with an uncertainty of 4×10^{-16} using a frequency link to international atomic time, J. Mod. Opt. **65**, 585 (2017).

[22] J. Lodewyck, S. Bilicki, E. Bookjans, J. Robyr, C. Shi, G. Vallet, R. L. Targat, D. Nicolodi, Y. Le Coq, J. Guéna, *et al.*, Optical to microwave clock frequency ratios with a nearly continuous strontium optical lattice clock, Metrologia **53**, 1123 (2016).

[23] I. R. Hill, R. Hobson, W. Bowden, E. M. Bridge, S. Donnellan, E. A. Curtis, and P. Gill, A low maintenance Sr optical lattice clock, J. Phys.: Conf. Ser. **723**, 012019 (2016).

[24] T. Kobayashi, D. Akamatsu, K. Hosaka, Y. Hisai, M. Wada, H. Inaba, T. Suzuyama, F. Hong, M. Yasuda, *et al.*, Demonstration of the nearly continuous operation of an ^{171}Yb optical lattice clock for half a year, Metrologia **57**, 065021 (2020).

[25] B. Zhang, Y. Huang, H. Zhang, Y. Hao, M. Zeng, H. Guan, and K. Gao, Progress on the $^{40}Ca^+$ ion optical clock, Chin. Phys. B **29**, 074209 (2020).

[26] See the Supplemental Material at http://link.aps.org/supplemental/10.1103/PhysRevApplied.19.064004 for additional details on the experimental apparatus and systematic shift evaluation and comparison experiment, which includes Refs. [4–7,25–42].

[27] Y. Huang, H. Guan, M. Zeng, L. Tang, and K. Gao, $^{40}Ca^+$ ion optical clock with micromotion-induced shifts below 1×10^{-18}, Phys. Rev. A **99**, 011401 (2019).

[28] K. Beloy, N. Hinkley, N. B. Phillips, J. A. Sherman, M. Schioppo, J. Lehman, A. Feldman, L. M. Hanssen, C. W. Oates, and A. D. Ludlow, Atomic Clock with 1×10^{-18} Room-Temperature Blackbody Stark Uncertainty, Phys. Rev. Lett. **113**, 260801 (2014).

[29] M. Doležal, P. Balling, P. B. R. Nisbet-Jones, S. A. King, J. M. Jones, H. A. Klein, P. Gill, T. Lindvall, A. E. Wallin, M. Merimaa, *et al.*, Analysis of thermal radiation in ion traps for optical frequency standards, Metrologia **52**, 842 (2015).

[30] P. Zhang, J. Cao, J. Yuan, D. Liu, Y. Yuan, Y. Wei, H. Shu, and X. Huang, Evaluation of blackbody radiation shift with 2×10^{-18} uncertainty at room temperature for a transportable $^{40}Ca^+$ optical clock, Metrologia **58**, 035001 (2021).

[31] D. Xiong, Q. Zhu, J. Wang, A. Zhang, C. Tian, B. Wang, L. He, Z. Xiong, and B. Lyu, Finite element analysis of blackbody radiation environment for an ytterbium lattice clock operated at room temperature, Metrologia **58**, 035005 (2021).

[32] D. J. Berkeland, J. D. Miller, J. C. Bergquist, W. M. Itano, and D. J. Wineland, Minimization of ion micromotion in a Paul trap, J. Appl. Phys. **83**, 5025 (1998).

[33] A. A. Madej, J. E. Bernard, P. Dubé, L. Marmet, and R. S. Windeler, Absolute frequency of the $^{88}Sr^+$ $5s^2S_{1/2}$–$4d^2D_{5/2}$ reference transition at 445 THz and evaluation of systematic shifts, Phys. Rev. A **70**, 012507 (2004).

[34] P. Dubé, A. A. Madej, Z. Zhou, and J. E. Bernard, Evaluation of systematic shifts of the $^{88}Sr^+$ single-ion optical frequency standard at the 10^{-17} level, Phys. Rev. A **87**, 023806 (2013).

[35] P. Dubé, A. A. Madej, M. Tibbo, and J. E. Bernard, High-Accuracy Measurement of the Differential Scalar Polarizability of a $^{88}Sr^+$ Clock Using the Time-Dilation Effect, Phys. Rev. Lett. **112**, 173002 (2014).

[36] J. Keller, H. L. Partner, T. Burgermeister, and T. E. Mehlstäubler, Precise determination of micromotion for trapped-ion optical clocks, J. Appl. Phys. **118**, 104501 (2015).

[37] H. S. Margolis, G. P. Barwood, G. Huang, H. A. Klein, S. N. Lea, K. Szymaniec, and P. Gill, Hertz-level measurement of the optical clock frequency in a single $^{88}Sr^+$ ion, Science **306**, 1355 (2004).

[38] Y. Huang, H. Guan, P. Liu, W. Bian, L. Ma, K. Liang, T. Li, and K. Gao, Frequency Comparison of Two $^{40}Ca^+$ Optical Clocks with an Uncertainty at the 10^{-17} Level, Phys. Rev. Lett. **116**, 013001 (2016).

[39] W. M. Itano, External-field shifts of the $^{199}Hg^+$ optical frequency standard, J. Res. Natl. Inst. Stand. Technol. **105**, 829 (2000).

[40] G. P. Barwood, H. S. Margolis, G. Huang, P. Gill, and H. A. Klein, Measurement of the Electric Quadrupole Moment of the $4d\,^2D_{5/2}$ Level in $^{88}Sr^+$, Phys. Rev. Lett. **93**, 133001 (2004).

[41] V. I. Yudin, A. V. Taichenachev, C. W. Oates, Z. W. Barber, N. D. Lemke, A. D. Ludlow, U. Sterr, C. Lisdat, and F. Riehle, Hyper-Ramsey spectroscopy of optical clock transitions, Phys. Rev. A **82**, 011804 (2010).

[42] B. Zhang, Y. Huang, Y. Hao, H. Zhang, M. Zeng, H. Guan, and K. Gao, Improvement in the stability of a $^{40}Ca^+$ ion optical clock using the Ramsey method, J. Appl. Phys. **128**, 143105 (2020).

[43] S. G. Porsev and A. Derevianko, Multipolar theory of blackbody radiation shift of atomic energy levels and its implications for optical lattice clocks, Phys. Rev. A **74**, 020502 (2006).

[44] E. Angstmann, V. Dzuba, and V. Flambaum, Frequency Shift of the Cesium Clock Transition due to Blackbody Radiation, Phys. Rev. Lett. **97**, 040802 (2006).

[45] K. Beloy, M. I. Bodine, T. Bothwell, S. M. Brewer, S. L. Bromley, J.-S. Chen, J.-D. Deschênes, S. A. Diddams, R. J. Fasano, T. M. Fortier, *et al.*, Frequency ratio measurements at 18-digit accuracy using an optical clock network, Nature **591**, 564 (2021).